

SCIENTIFIC REPORTS

OPEN

Five-partite entanglement generation between two optical frequency combs in a quasi-periodic $\chi^{(2)}$ nonlinear optical crystal

Guangqiang He^{1,2,3}, Yu Sun¹, Linxi Hu¹, Renhui Zhang¹, Xikun Chen¹ & Jindong Wang⁴

We theoretically prove five-partite entanglement can be produced among modes of two simultaneously generated optical frequency combs via second-order nonlinear interaction in a designed periodically poled lithium niobate (PPLN) crystal. An extendible model is proposed to analyze the entanglement characteristics of generated comb modes by applying van Loock and Furusawa criteria. Our proposal provides a potential approach for generating multipartite entangled states, the so-called cluster states, which are the key resources for quantum computation. Moreover, simultaneous generation of two entangled combs can provide much higher efficiency to generate cluster states.

Quantum entanglement is at the central part of applications such as quantum computation and quantum communication, such as quantum teleportation^{1–3}, quantum key distribution⁴, quantum secure direct communication^{5–7}, quantum machine learning⁸, and so on. To experimentally implement quantum computation, scalability is one of the most essential requirements⁹. Thus a so-called one-way quantum computer model¹⁰, in which quantum computation resource is provided by cluster states¹¹, was proposed for the requirement. A cluster state is a multipartite entangled state in which any algorithm can be implemented by one-particle measurements only. Motivated by this discovery, a large number of works related to cluster states have been carried out^{9, 12–20}. Various generation methods of cluster states are investigated, such as using beta-barium borate (BBO)¹³, cavity quantum electrodynamics (QED) techniques¹⁵, and optical frequency combs (OFCs)^{9, 18–20}. Among these works, resorting to optical frequency combs is quite appealing. Some interesting works have been proposed about entanglement generated in optical combs. It is shown that optical-frequency combs are formed by the interaction between a cavity mode and a continuous-wave two-tone driving laser consisting of a pump field and a seed field via quantum dot-induced strong nonlinearity²¹. A large-scale quantum entanglement between two comb modes has very recently been explored in an interacting semiconductor quantum dot-photon molecule system²².

OFCs have already found its way to applications such as precision spectroscopy, frequency transfer, astronomical spectral calibration, and generation of low-phase-noise microwave and radio frequency oscillators²³. Initially, optical frequency combs were produced by mode-locked femtosecond laser²³, it is stable but bulky and complex. For the sake of miniaturization, microresonators have been proposed and experimentally demonstrated to generate optical frequency combs based on the cascaded four-wave mixing (FWM), allowing considerable reduction of complexity, size and power consumption^{24, 25}. FWM is third-order nonlinear effect and its conversion efficiency is much less than second-order nonlinear effects such as second-harmonic generation (SHG) and sum-frequency generation (SFG). Thus optical frequency combs generated via second-order nonlinearity have drawn growing attention. Iolanda *et al.*²⁶ and Ville *et al.*²⁷ have shown that two OFCs can be produced simultaneously by cascaded SHG and SFG. In their works, different features and generation regimes are investigated, good spectral quality is also shown. Inspired by their works, we proposed a novel model to analyze the entanglement characteristics of the two combs in this paper. Simultaneous generation of two entangled combs can provide much higher efficiency

¹State Key Laboratory of Advanced Optical Communication Systems and Networks, Electronic Engineering Department, Shanghai Jiao Tong University, Shanghai, 200240, China. ²State Key Laboratory of Precision Spectroscopy, East China Normal University, Shanghai, 200062, China. ³State Key Laboratory of Information Security, Institute of Information Engineering, Chinese Academy of Sciences, Beijing, 100093, China. ⁴Guangdong Provincial Key Laboratory of Quantum Engineering and Quantum Materials, South China Normal University, Guangzhou, 510006, PR China. Correspondence and requests for materials should be addressed to G.H. (email: gqhe@sjtu.edu.cn) or J.W. (email: wangjd@scnu.edu.cn)

Received: 6 June 2017
Accepted: 17 July 2017
Published online: 22 August 2017

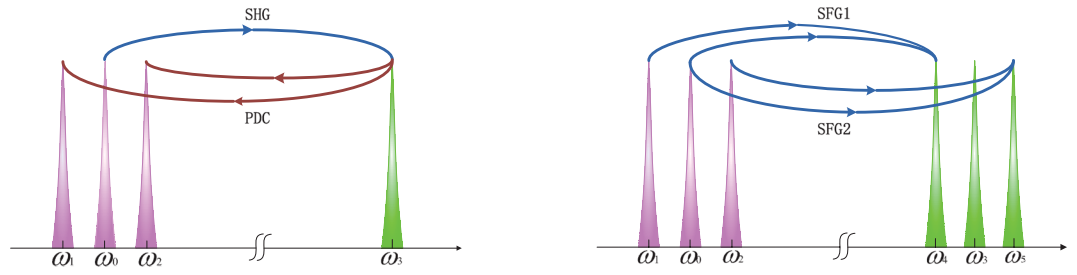


Figure 1. Second-harmonic generation (SHG) with cascaded down-conversion (PDC) process gives rise to the frequency components ω_3, ω_1 and ω_2 , which in turns leads to two sum-frequency processes (SFG1, SFG2) and generate another two subharmonic components ω_4, ω_5 .

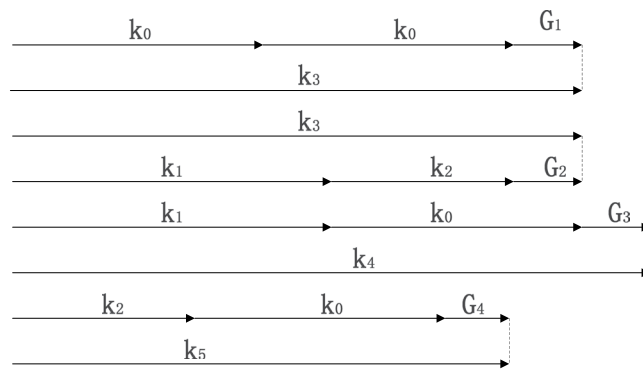


Figure 2. The quasi-phase matching scheme for the cascaded nonlinear processes.

to generate cluster states, making an important step for quantum computation. Without loss of generality, we simplify the two combs with three modes in each comb, thus there are six modes in total.

The rest of this paper is arranged as follows. In result and discussion, system model and output fluctuation spectra are given as two parts. First, we describe the physical model for the generation of five-partite entanglement, then derive the main values and fluctuations of the output fields in system model. In output fluctuation spectra, the entanglement characteristics of the modes in two frequency combs are investigated. In method, we introduce the principle of designing the model and analyzing the four-partite entanglement.

Results and Discussion

System Model. In this model, two output frequency combs consisted of six modes are generated by cascaded second-order nonlinear processes as shown in Fig. 1. First, a pump with frequency ω_0 generates the beam with frequency ω_3 through a second-harmonic generation. Then, two beams with frequency ω_1 and ω_2 are generated by a down-conversion process. Last, two beams with frequency ω_4 and ω_5 are generated by two sum-frequency processes.

According to the above nonlinear processes, The energy conversion and phase-matching conditions can be written as follows:

$$SHG: \omega_0 + \omega_0 = \omega_3, k_0 + k_0 + G_1 = k_3, \tag{1}$$

$$PDC: \omega_1 + \omega_2 = \omega_3, k_1 + k_2 + G_2 = k_3, \tag{2}$$

$$SFG1: \omega_0 + \omega_1 = \omega_4, k_0 + k_1 + G_3 = k_4, \tag{3}$$

$$SFG2: \omega_0 + \omega_2 = \omega_5, k_0 + k_2 + G_4 = k_5. \tag{4}$$

$k_i (i=0, 1, 2, 3, 4, 5)$ are the corresponding wave vectors of the six output modes with frequency $\omega_i (i=0, 1, 2, 3, 4, 5)$. G_1, G_2, G_3, G_4 are the four reciprocals needed to compensate the phase mismatching. The quasiphasematching sketch is plotted in Fig. 2.

To obtain the reciprocal-lattice vector for corresponding quasiphasemismatch, an optical superlattice (OS) is needed, and the superlattice can be designed using a dual-grid method. Due to Iolanda *et al.*'s work²⁶, we set the six wavelengths with frequency $\omega_i (i=0, \dots, 5)$ at 1064.45, 1065.54, 1063.36, 532.225, 532.50, 531.95 nm, respectively, and the temperature is 39.5 °C. The tiling vectors of the OS are calculated to be 1.739, 1.740, 1.735,

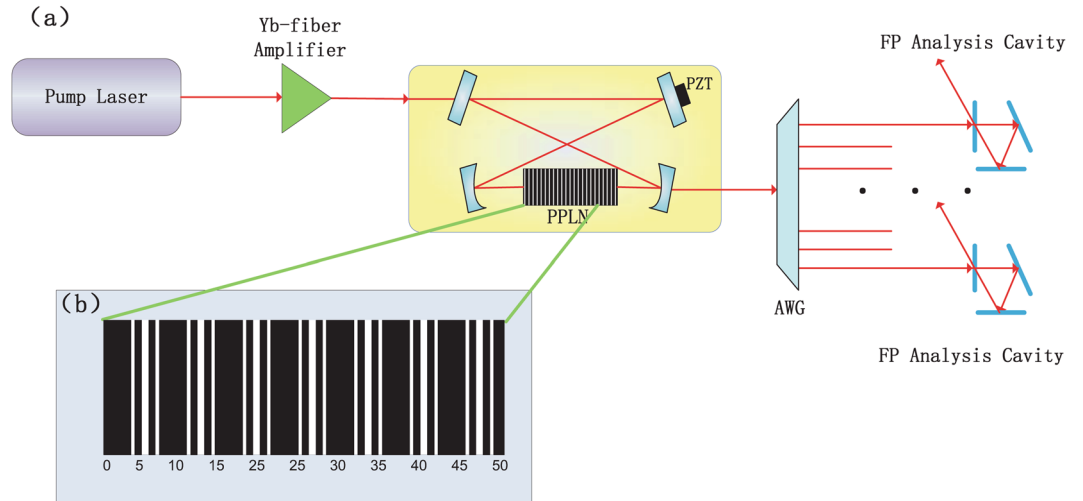


Figure 3. Experimental setup. (a) A four-mirrors travelling wave cavity, with a PPLN crystal, is pumped by an amplified cw laser. The nonlinear cavity output beams are separated by an arrayed waveguide grating (AWG) and then analyzed by the Fabry-Perot (FP) analysis cavities. (b) The structure of the PPLN OS.

1.742 μm . The structure of the PPLN OS is shown in Fig. 3(b), where the index of refraction of the black blocks is negative and the index of refraction of the white blocks is positive. The unit of length in Fig. 3b is micrometer.

Since the structure of the PPLN crystal is obtained, we design a schematic diagram of physical system as shown in Fig. 3. The system is pumped by a continuous-wave pump laser at 1064.45 nm, amplified by a Yb: fiber amplifier. Then the pump beam enters the cavity through a plane coupling mirror, while other mirrors are high-reflectivity. The high-reflectivity plane mirror is mounted on a piezoelectric actuator (PZT) for cavity length control and the designed PPLN crystal is placed between the two curved mirrors. The nonlinear processes give rise to the output frequency combs, which will finally be separated by an arrayed waveguide grating (AWG) and analyzed by the Fabry-Perot (FP) analysis cavities.

Due to the nonlinear processes proposed above, the interaction Hamiltonian H_i for the nonlinear processes, the Hamiltonian for the pump beam H_p are as follow:

$$H_p = i\hbar a_0^\dagger \varepsilon + H.c. , \tag{5}$$

$$H_i = i\hbar(\kappa_1 a_0 a_0 a_3^\dagger + \kappa_2 a_1^\dagger a_2^\dagger a_3 + \kappa_3 a_0 a_1 a_4^\dagger + \kappa_4 a_0 a_2 a_5^\dagger) + H.c. \tag{6}$$

where $\kappa_i (i = 1, 2, 3, 4)$ are the dimensionless nonlinear coupling coefficients of the nonlinear processes, \hat{a}_i are annihilation operators of the modes with frequency ω_i .

An optical oscillator is an open system since it not only exhibits intrinsic scattering loss with a photon decay rate of γ_{k0} (for mode k), but also couples waves to the coupling waveguide with an external coupling rate of γ_{kc} . In order to describe such an open system, we present the loss and out-coupling terms as:

$$L_k \hat{\rho} = \gamma_k (2a_k \hat{\rho} a_k^\dagger - a_k^\dagger a_k \hat{\rho} - \hat{\rho} a_k^\dagger a_k). \tag{7}$$

where $\hat{\rho}$ stands for the density matrix of system and $\gamma_k = \gamma_{kc} + \gamma_{k0}$ represents the damping rate of the loaded cavity. Then the output field is determined by the well-known input-output relation given as ref. 28

$$b_{out} - b_{in} = \sqrt{\gamma} a. \tag{8}$$

in which b is the boson annihilation operator for the bath field outside the cavity.

As for the system model presented previously, whole procedure could be governed by the following master equation:

$$\frac{\partial \hat{\rho}}{\partial t} = -\frac{i}{\hbar} [H_p + H_i, \hat{\rho}] + \sum_{k=0}^5 L_k \hat{\rho}. \tag{9}$$

The above master equation can be converted into the equivalent c -number Fockker-Planck equation in P representation, which may be written as a completely equivalent stochastic differential equation:

$$\frac{\partial \alpha}{\partial t} = F + B\eta, \tag{10}$$

where

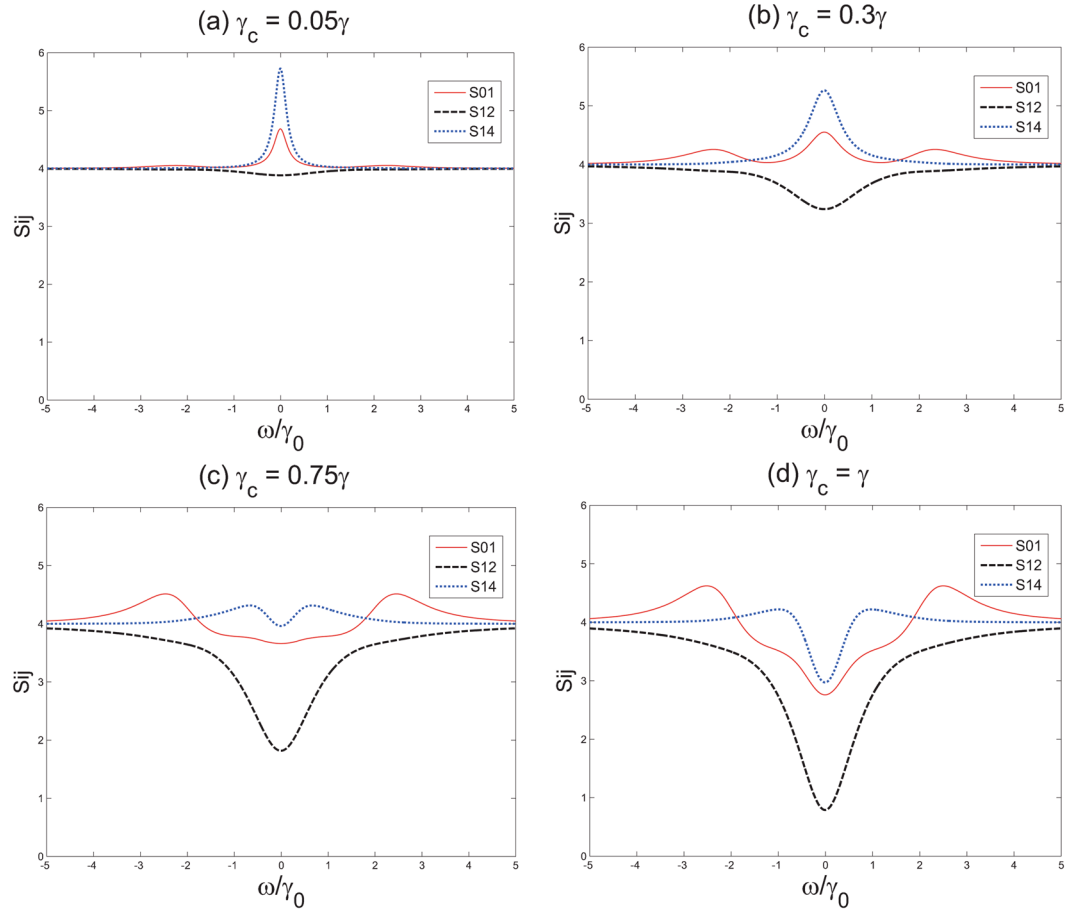


Figure 4. Four variances versus frequency of pump plots when γ_c/γ is 0.05, 0.3, 0.7, 1. The pump power is fixed at $1.5\epsilon_{th}$.

$$\alpha = [\alpha_0, \alpha_1, \alpha_2, \alpha_3, \alpha_4, \alpha_5, \alpha_0^*, \alpha_1^*, \alpha_1^*, \alpha_3^*, \alpha_4^*, \alpha_5^*], \tag{11}$$

$$\eta = [\eta_1, \eta_2, \eta_3, \eta_4, \eta_5, \eta_6, \eta_7, \eta_8, \eta_9, \eta_{10}, \eta_{11}, \eta_{12}], \tag{12}$$

$$F = \begin{bmatrix} f \\ f^* \end{bmatrix}, \tag{13}$$

$$f = \begin{pmatrix} \gamma_0\alpha_0 - \varepsilon + 2\kappa_1\alpha_0^*\alpha_3 + \nu_3\alpha_1^*\alpha_4 + \kappa_4\alpha_2^*\alpha_5 \\ \gamma_1\alpha_1 - \kappa_2\alpha_2^*\alpha_3 + \kappa_3\alpha_0^*\alpha_4 \\ \gamma_2\alpha_2 - \kappa_2\alpha_1^*\alpha_3 + \kappa_4\alpha_0^*\alpha_5 \\ \gamma_3\alpha_3 - \kappa_1\alpha_0\alpha_0 + \kappa_2\alpha_1\alpha_2 \\ \gamma_4\alpha_4 - \kappa_3\alpha_0\alpha_1 \\ \gamma_5\alpha_5 - \kappa_4\alpha_0\alpha_2 \end{pmatrix}. \tag{14}$$

$\alpha_i = \bar{\alpha}_i + \delta\alpha_i$, where α_i are the fields with frequency ω_i , $\bar{\alpha}_i$ are mean values of α_i , and $\delta\alpha_i$ are the fluctuations of the fields. $\eta_i (i = 1, \dots, 12)$ are the real noise terms. Matrix B could be obtained by the relationship $D = BB^T$. D matrix we introduced here stands for the diffusion matrix, which is given by

$$D = \begin{pmatrix} d & 0 \\ 0 & d^* \end{pmatrix}, \tag{15}$$

where d is given by

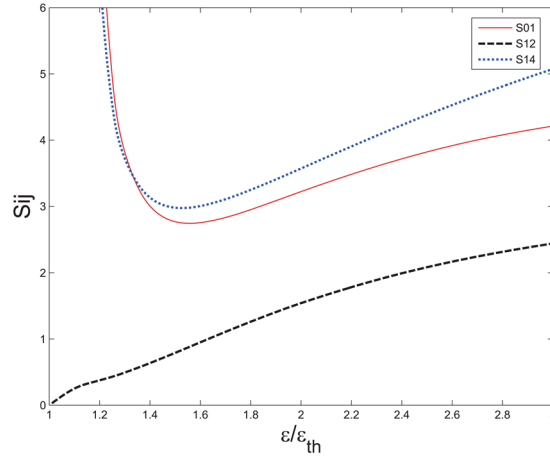


Figure 5. The minimum variance as a function of pump power. The external coupling coefficient is fixed at $\gamma_c = \gamma$.

$$d = \begin{pmatrix} -2\kappa_1\alpha_3 & -\kappa_3\alpha_4 & -\kappa_4\alpha_5 & 0 & 0 & 0 \\ -\kappa_3\alpha_4 & 0 & \kappa_2\alpha_3 & 0 & 0 & 0 \\ -\kappa_3\alpha_5 & \kappa_2\alpha_3 & 0 & 0 & 0 & 0 \\ 0 & 0 & 0 & 0 & 0 & 0 \\ 0 & 0 & 0 & 0 & 0 & 0 \\ 0 & 0 & 0 & 0 & 0 & 0 \end{pmatrix}. \tag{16}$$

In order to obtain the steady-state solutions of the above processes, the noise terms and all the fluctuations can be neglected; thus the equations for the mean values of the fields can be written as:

$$\frac{\partial \delta \bar{\alpha}_0}{\partial t} = \gamma_0 \bar{\alpha}_0 - \varepsilon + 2\kappa_1 \bar{\alpha}_0^* \bar{\alpha}_3 + \kappa_3 \bar{\alpha}_1^* \bar{\alpha}_4 + \kappa_4 \bar{\alpha}_2^*, \tag{17}$$

$$\frac{\partial \delta \bar{\alpha}_1}{\partial t} = \gamma_1 \bar{\alpha}_1 - \kappa_2 \bar{\alpha}_2^* \bar{\alpha}_3 + \kappa_3 \bar{\alpha}_0^* \bar{\alpha}_4, \tag{18}$$

$$\frac{\partial \delta \bar{\alpha}_2}{\partial t} = \gamma_2 \bar{\alpha}_2 - \kappa_2 \bar{\alpha}_1^* \bar{\alpha}_3 + \kappa_4 \bar{\alpha}_0^* \bar{\alpha}_5, \tag{19}$$

$$\frac{\partial \delta \bar{\alpha}_3}{\partial t} = \gamma_3 \bar{\alpha}_3 - \kappa_1 \bar{\alpha}_0 \bar{\alpha}_0 + \kappa_2 \bar{\alpha}_1 \bar{\alpha}_2, \tag{20}$$

$$\frac{\partial \delta \bar{\alpha}_4}{\partial t} = \gamma_4 \bar{\alpha}_4 - \kappa_3 \bar{\alpha}_0 \bar{\alpha}_1, \tag{21}$$

$$\frac{\partial \delta \bar{\alpha}_5}{\partial t} = \gamma_5 \bar{\alpha}_5 - \kappa_4 \bar{\alpha}_0 \bar{\alpha}_2. \tag{22}$$

Firstly we get the steady-state solution by setting the $\frac{\partial \delta \bar{\alpha}_i}{\partial t} = 0$. Though the pump threshold can be obtained in analytical solution, it is too complex. So we choose to get the pump threshold by a numerical method. For example, when $\gamma_0 = 0.01, \gamma_1 = 0.01, \gamma_2 = 0.01, \gamma_3 = 0.01, \gamma_4 = 0.01, \gamma_5 = 0.01, \kappa_1 = 0.03, \kappa_2 = 0.03, \kappa_3 = 0.01, \kappa_4 = 0.01$, the threshold is $\varepsilon_{th} = 0.003243$. Notice that, when the pump wave power is below the threshold, there would be no steady solution for output waves. Thus we only investigate the entanglement characteristics above the threshold. Since the mean values of the fields in the cavity are obtained, they can be used to linearize the classical motion equations for the fields in the cavity to obtain the equations of the fluctuations of the fields:

$$\frac{\partial \delta \bar{\alpha}}{\partial t} = M \delta \bar{\alpha} + B \eta, \tag{23}$$

in which $\delta \bar{\alpha} = [\delta \alpha_0, \delta \alpha_1, \delta \alpha_2, \delta \alpha_3, \delta \alpha_4, \delta \alpha_5, \delta \alpha_0^*, \delta \alpha_1^*, \delta \alpha_2^*, \delta \alpha_3^*, \delta \alpha_4^*, \delta \alpha_5^*]^T$. M is the drift matrix given by

$$M = \begin{pmatrix} m_1 & m_2 \\ m_2^* & m_1^* \end{pmatrix}, \tag{24}$$

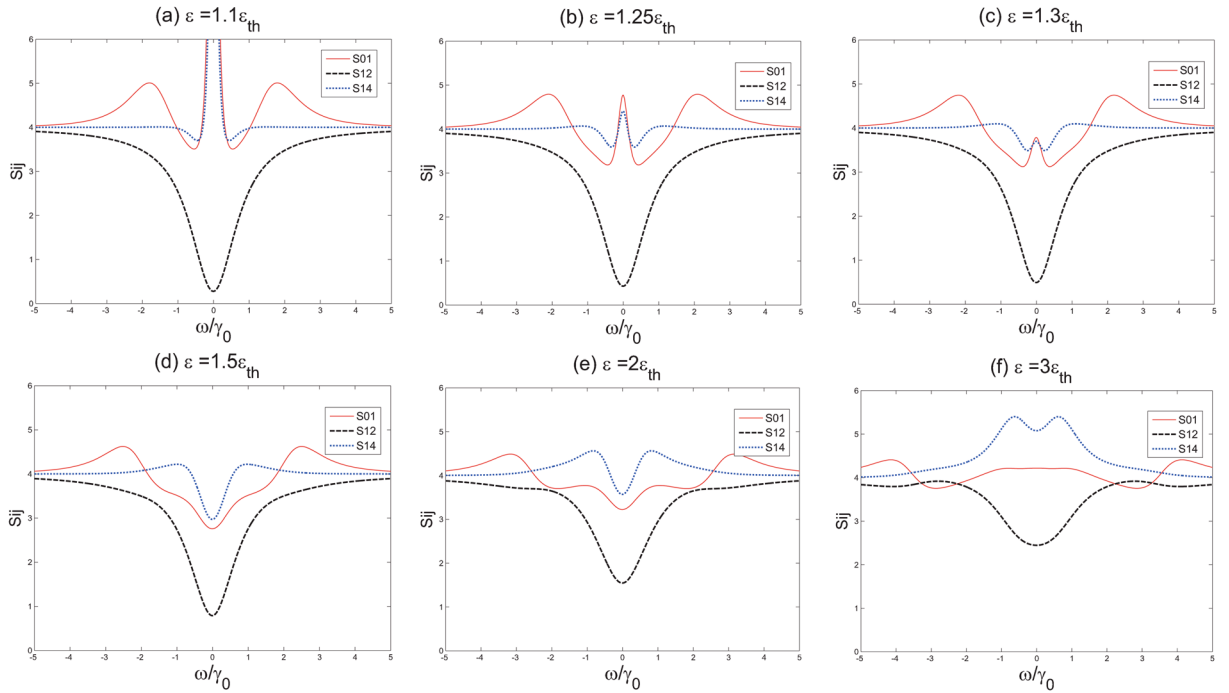


Figure 6. Extracavity variance versus frequency of pump power. The external coupling coefficient is fixed at: $\gamma_c = \gamma$.

where m_1 and m_2 is

$$m_1 = \begin{pmatrix} -\gamma_0 & 0 & 0 & -2\kappa_1\bar{\alpha}_0^* & -\kappa_3\bar{\alpha}_1^* & -\kappa_4\bar{\alpha}_2^* \\ 0 & -\gamma_1 & 0 & \kappa_2\bar{\alpha}_2^* & -\kappa_3\bar{\alpha}_0^* & 0 \\ 0 & 0 & -\gamma_2 & \kappa_2\bar{\alpha}_1^* & 0 & -\kappa_4\bar{\alpha}_0^* \\ 2\kappa_1\bar{\alpha}_0 & -\kappa_2\bar{\alpha}_2 & -\kappa_2\bar{\alpha}_1 & -\gamma_3 & 0 & 0 \\ \kappa_3\bar{\alpha}_1 & \kappa_3\bar{\alpha}_0 & 0 & 0 & -\gamma_4 & 0 \\ \kappa_4\bar{\alpha}_2 & 0 & \kappa_4\bar{\alpha}_0 & 0 & 0 & -\gamma_5 \end{pmatrix}, \tag{25}$$

$$m_2 = \begin{pmatrix} -2\kappa_1\bar{\alpha}_3 & -\kappa_3\bar{\alpha}_4 & -\kappa_4\bar{\alpha}_5 & 0 & 0 & 0 \\ -\kappa_3\bar{\alpha}_4 & 0 & \kappa_2\bar{\alpha}_3 & 0 & 0 & 0 \\ -\kappa_4\bar{\alpha}_5 & \kappa_2\bar{\alpha}_3 & 0 & 0 & 0 & 0 \\ 0 & 0 & 0 & 0 & 0 & 0 \\ 0 & 0 & 0 & 0 & 0 & 0 \\ 0 & 0 & 0 & 0 & 0 & 0 \end{pmatrix}. \tag{26}$$

For the validity of linearised quantum-fluctuation analysis, the quantum-fluctuation must be small enough compared with mean values. If the requirement that the real parts of the eigenvalues of $-M$ stay non-negative is satisfied, the fluctuation equations will describe an Ornstein-Uhlenbeck process²⁹, for which the intracavity spectral correlation matrix is given by

$$S(\omega) = (-M + i\omega I)^{-1} D (-M^T - i\omega I)^{-1}. \tag{27}$$

We introduce the quadrature operators for each mode in order to discuss the five-partite entanglement:

$$X_k = a_k + a_k^\dagger, \tag{28}$$

$$Y_k = -i(a_k - a_k^\dagger), \tag{29}$$

with a commutation relationship of $[X_k, Y_k] = 2i$. Thus we know that $V(X_k) \leq 1$ could stands for the squeezed state based on our operator definition. $V(A) = \langle A^2 \rangle - \langle A \rangle^2$ indicates the variance of operator A .

The output fields is determined by the well-known input-output relations Eq. 8. In particular, the spectral variances and covariances have the general form

$$S_{X_i}^{out}(\omega) = 1 + 2\gamma_c S_{X_i}(\omega), \tag{30}$$

$$S_{X_i, X_j}^{out}(\omega) = 2\gamma_c S_{X_i, X_j}(\omega), \quad (31)$$

Y quadratures have the similar expressions.

Multipartite entanglement criteria is given by the Van Loock and Furusawa (VLF)³⁰. In our discussion, we consider Fokker-Planck equation in P representation and then analyse the entanglement condition that van Loock and Furusawa criteria are violated simultaneously. By using the above quadrature definitions, the five-partite criteria is given by

$$S_{01} = V(X_0 - X_1) + V(Y_0 + Y_1 + g_2 Y_2 + g_3 Y_3 + g_4 Y_4 + g_5 Y_5) \geq 4, \quad (32)$$

$$S_{12} = V(X_1 - X_2) + V(g_0 Y_0 + Y_1 + Y_2 + g_3 Y_3 + g_4 Y_4 + g_5 Y_5) \geq 4, \quad (33)$$

$$S_{14} = V(X_1 - X_4) + V(g_0 Y_0 + Y_1 + g_2 Y_2 + g_3 Y_3 + Y_4 + g_5 Y_5) \geq 4, \quad (34)$$

$$S_{25} = V(X_2 - X_5) + V(g_0 Y_0 + g_1 Y_1 + Y_2 + g_3 Y_3 + g_4 Y_4 + Y_5) \geq 4. \quad (35)$$

in which $g_k (k=0, \dots, 5)$ are arbitrary real parameters that are used to optimize the violation of these inequalities. Considering the frequency component of ω_3 is generated by SHG, it is hardly to entangle with other modes, we only investigate entanglement characteristics among other five mode. According to the symmetry between ω_1 and ω_2 , we choose to investigate S_{01} , S_{12} and S_{14} in our rest analysis.

Output Fluctuation Spectra. According to Eqs [17–22], the stable solution is completely determined by three parameters: the total damping rate γ , the coupling coefficient κ , and the pumping power ε , which in turn determines the drift matrix M, the diffusion matrix D, and the intracavity spectral correlation matrix S. In addition, we also conclude that the parameter γ_c plays a role in the spectral correlation matrices according to Eqs [30 and 31]. In the following work, we will vary these parameters to investigate the entanglement.

To begin with, we fix κ , γ and ε - the three parameters that governs the evolution in the cavity, and vary the γ_c/γ ratio to investigate its influence on the entanglement. To satisfy the validity of the linearization method and calculate the quantum correlation spectra, the parameters should be chosen properly. Therefore, we set $\gamma_0 = 0.01$, $\gamma_1 = 0.003$, $\gamma_2 = 0.003$, $\gamma_3 = 0.01$, $\gamma_4 = 0.01$, $\gamma_5 = 0.01$, $\kappa_1 = 0.03$, $\kappa_2 = 0.03$, $\kappa_3 = 0.01$, $\kappa_4 = 0.01$. With above parameters, we plot the minimum of the variances versus the analysis frequency normalized to γ in Fig. 4 when γ_c takes a portion of 0.05, 0.3, 0.75 and 1.

From Fig. 4, we can see that when $\gamma_c/\gamma = 0.05$, there is no entanglement between any two frequency modes. As we increase the out-coupling coefficient, the three frequencies in the first comb begin to entangle with each other. When $\gamma_c/\gamma = 0.75$, the ω_1 and ω_2 , which are respectively in two different combs, begin to entangle. And eventually when we set the portion to the $\gamma_c/\gamma = 1$, the degree of entanglement is the largest compared with other case. Thus, we conclude that the entanglement among output modes increases as the ratio γ_c/γ increases. This can be explained that the higher portion the coupling coefficient takes, the less consumed entangled pairs are wasted in the internal loss.

In order to investigate the effect the pump power brings to the degree of entanglement, we firstly set the $\gamma_0 = 0$ which means no intracavity loss in this part of discussion. With our previous discussion, the variance S_i as a function of ω/γ is merely determined by the parameter $\varepsilon/\varepsilon_{th}$ while choose proper κ and γ . We plot the minimum variance throughout the noise power spectrum as a function of the pump power which has been normalized by ε_{th} in Fig. 5. We plot the minimum variance versus frequency under different pumping power in Fig. 6.

It can be inferred from Fig. 5 that the variance of S_{01} and S_{14} would first decrease as the pump power increasing and reach their minimum values when $\varepsilon = 1.5\varepsilon_{th}$ around. Then S_{01} and S_{14} would ascend with the pump power while S_{12} increases as the pump power since the beginning. Considering that S_{01} and S_{14} are the short slabs of the entanglement model, we conclude that the $1.5\varepsilon_{th}$ is the best pump power in our case. That explains why we choose $\varepsilon = 1.5\varepsilon_{th}$ in previous investigation.

In conclusion, we propose the theoretical model for the five-entanglement among modes of two optical frequency combs. By solving Fokker-Planck equation in P representation, we analysed the entanglement case where Van Loock and Furusawa criteria are violated. We analytically find that the intensity of entanglement is completed influenced by the $\varepsilon/\varepsilon_{th}$, ω/γ , and γ_c/γ . The results would offer a new path for the future study for entanglement over optical frequency combs generated via second-order nonlinear interaction.

Method

We design the PPLN crystal using the so-called generalized dual grid method (DGM), which will phase match the four nonlinear processes. In this method, a dual structure, called dual grid, which contains all the topological information required to build the quasi-crystal is constructed and transformed to a quasi-crystal.

We analyze the entanglement case based on the Van Loock and Furusawa criteria. First, we obtain the main equation and transform it into Fokker-Planck equation. After we get the steady-solution of the above equations, we can obtain the equations of the fluctuations of the fields. Then, we calculate the spectral variances and covariances which will be applied into the Van Loock and Furusawa criteria. Finally, the influences of $\varepsilon/\varepsilon_{th}$, ω/γ , and γ_c/γ on the intensity of entanglement are analysed.

Our analysis method is also suitable for other types of entanglement, such as multi-partite GHZ state and logic-qubit entanglement, as long as the nonlinear processes are given we can derive the Hamiltonian expressions, then we can analyze the entanglement characteristics according to the method we propose above.

References

- Li, T. C. & Yin, Z. Q. Quantum superposition, entanglement, and state teleportation of a microorganism on an electromechanical oscillator. *Sci. Bull.* **61**, 163–171 (2016).
- Ai, Q. Toward quantum teleporting living objects. *Sci. Bull.* **61**, 110–111 (2016).
- Tan, Y. G. Quantum key distribution with prepare-and-measure Bell test. *Sci. Rep.* **6**, 35032 (2016).
- Li, J., Yang, Y. G., Chen, X. B., Zhou, Y. H. & Shi, W. M. Practical quantum private database queries based on passive Round-Robin Differential phase-shift quantum key distribution. *Sci. Rep.* **6**, 31738 (2016).
- Long, G. L. & Liu, X. S. Theoretically efficient high-capacity quantum key distribution scheme. *Phys. Rev. A* **65**, 032302 (2002).
- Deng, F. G., Long, G. L. & Liu, X. S. Two-step quantum direct communication protocol using the Einstein-Podolsky-Rosen Pair block. *Phys. Rev. A* **68**, 042317 (2003).
- Zhang, W. *et al.* Quantum secure direct communication with quantum memory. *Phys. Rev. Lett.* **118**, 220501 (2017).
- Sheng, Y. B. & Zhou, L. Distributed secure quantum machine learning. *Sci. Bull.*, doi:10.1016/j.scib.2017.06.007.
- Pysher, M., Miwa, Y., Shahrokhshahi, R., Bloomer, R. & Pfister, O. Parallel Generation of Quadripartite Cluster Entanglement in the Optical Frequency Comb. *Phys. Rev. Lett.* **107**, 030505 (2011).
- Raussendorf, R. & Briegel, H. J. A One-Way Quantum Computer. *Phys. Rev. Lett.* **86**, 5188 (2000).
- Briegel, H. J. & Raussendorf, R. Persistent Entanglement in Arrays of Interacting Particles. *Phys. Rev. Lett.* **86**, 910 (2000).
- Raussendorf, R., Browne, D. E. & Briegel, H. J. Measurement-based quantum computation on cluster states. *Phys. Rev. A* **68**, 022312 (2003).
- Zhao, Z. *et al.* Experimental demonstration of five-photon entanglement and open-destination teleportation. *Nature* **430**, 54–58 (2004).
- Scarani, V., Acin, A., Schenck, E. & Aspelmeyer, M. Nonlocality of cluster states of qubits. *Phys. Rev. A* **71**, 042325 (2005).
- Dong, P., Xue, Z.-Y., Yang, M. & Cao, Z.-L. Generation of cluster states. *Phys. Rev. A* **73**, 033818 (2006).
- Rosenkranz, M. & Jaksch, D. Parameter estimation with cluster states. *Phys. Rev. A* **79**, 022103 (2009).
- Weinstein, Y. S., Feldman, J., Robins, J., Zukus, J. & Gilbert, G. Superoperator analysis of entanglement in a four-qubit cluster state. *Phys. Rev. A* **85**, 032324 (2012).
- Chen, M., Menicucci, N. C. & Pfister, O. Experimental Realization of Multipartite Entanglement of 60 modes of a Quantum Optical Frequency Comb. *Phys. Rev. Lett.* **112**, 120505 (2014).
- Menicucci, N. C., Flammia, S. T. & Pfister, O. One-Way Quantum Computing in the Optical Frequency Comb. *Phys. Rev. Lett.* **101**, 130501 (2008).
- Roslund, J., de Araujo, R. M., Jiang, S., Fabre, C. & Treps, N. Wavelength-multiplexed quantum networks with ultrafast frequency combs. *Nature Photon* **8**, 340 (2013).
- Li, J., Yu, R., Ding, C., Wang, Wei & Wu, Y. Optical-frequency-comb generation and entanglement with low-power optical input in a photonic molecule. *Phys. Rev. A* **90**, 033830 (2014).
- Li, J., Yu, R., Ma, J. & Wu, Y. All-optical control of optical frequency combs via quantum interference effects in a single-emitter-microcavity system. *Phys. Rev. A* **91**, 063834 (2015).
- Jones, D. J. *et al.* Carrier-Envelope Phase Control of Femtosecond Mode-Locked Lasers and Direct Optical Frequency Synthesis. *Science* **288**, 1933 (2000).
- Del'Haye, P. A. *et al.* Optical frequency comb generation from a monolithic microresonator. *Nature* **450**, 1214–1217 (2007).
- Savchenkov, A. A. *et al.* Tunable Optical Frequency Comb with a Crystalline Whispering Gallery Mode Resonator. *Phys. Rev. Lett.* **101**, 093902 (2008).
- Ricciardi, I. *et al.* Frequency comb generation in quadratic nonlinear media. *Phys. Rev. A* **91**, 063839 (2015).
- Ulvila, V., Phillips, C. R., Halonen, L. & Vainio, M. Spectral characterization of a frequency comb based on cascaded quadratic nonlinearities inside an optical parametric oscillator. *Phys. Rev. A* **92**, 033816 (2015).
- Gardiner, C. W. & Collett, M. J. Input and output in damped quantum systems: Quantum stochastic differential equations and the master equation. *Phys. Rev. A* **31**, 3761 (1985).
- Gardiner, C. *Stochastic methods* (Springer-Verlag, Berlin-Heidelberg-New York-Tokyo, 1985).
- van Loock, P. & Furusawa, A. Detecting genuine multipartite continuous-variable entanglement. *Phys. Rev. A* **67**, 052315 (2003).

Acknowledgements

This work is supported by the National Natural Science Foundation of China (Grant Nos 61475099, 61102053), Program of State Key Laboratory of Quantum Optics and Quantum Optics Devices (Nos KF201405, KF201701), Open Fund of IPOC (BUPT) (No: IPOC2015B004), Program of State Key Information Security (No. 2016-MS-05).

Author Contributions

G.H. generated the idea and led the project. G.H. designed the experiment setup. R.Z. and L.H. designed the crystal. X.C. and Y.S. did theoretical derivation. Y.S. analyzed the data. J.W. gave some constructive suggestions about the scheme. All authors discussed the results and contributed to the preparation of the manuscript.

Additional Information

Competing Interests: The authors declare that they have no competing interests.

Publisher's note: Springer Nature remains neutral with regard to jurisdictional claims in published maps and institutional affiliations.



Open Access This article is licensed under a Creative Commons Attribution 4.0 International License, which permits use, sharing, adaptation, distribution and reproduction in any medium or format, as long as you give appropriate credit to the original author(s) and the source, provide a link to the Creative Commons license, and indicate if changes were made. The images or other third party material in this article are included in the article's Creative Commons license, unless indicated otherwise in a credit line to the material. If material is not included in the article's Creative Commons license and your intended use is not permitted by statutory regulation or exceeds the permitted use, you will need to obtain permission directly from the copyright holder. To view a copy of this license, visit <http://creativecommons.org/licenses/by/4.0/>.

© The Author(s) 2017